


## ARTICLE



# Ocular microbiota promotes pathological angiogenesis and inflammation in sterile injury-driven corneal neovascularization

Hyun Ju Lee<sup>1,7</sup>, Chang Ho Yoon<sup>1,2,7</sup>, Hyeon Ji Kim<sup>1</sup>, Jung Hwa Ko<sup>1</sup>, Jin Suk Ryu<sup>1</sup>, Dong Hyun Jo<sup>3</sup>, Jeong Hun Kim<sup>2,4</sup>, Donghyun Kim<sup>5,6</sup> and Joo Youn Oh<sup>1,2</sup> 

© The Author(s), under exclusive licence to Society for Mucosal Immunology 2022

Microbiota promotes or inhibits the pathogenesis of a range of immune-mediated disorders. Although recent studies have elucidated the role of gut microbiota in ocular disease, the effect of ocular microbiota remains unclear. Herein, we explored the role of ocular commensal bacteria in non-infectious corneal inflammation and angiogenesis in a mouse model of suture-induced corneal neovascularization. Results revealed that the ocular surface harbored a microbial community consisting mainly of *Actinobacteria*, *Firmicutes* and *Proteobacteria*. Elimination of the ocular commensal bacteria by oral broad-spectrum antibiotics or topical fluoroquinolone significantly suppressed corneal inflammation and neovascularization. Disease amelioration was associated with reduced numbers of CD11b<sup>+</sup>Ly6C<sup>+</sup> and CD11b<sup>+</sup>Ly6G<sup>+</sup> myeloid cells, not Foxp3<sup>+</sup> regulatory T cells, in the spleen, blood, and draining lymph nodes. Therapeutic concentrations of fluoroquinolone, however, did not directly affect immune cells or vascular endothelial cells. In addition, data from a clinical study showed that antibiotic treatment in combination with corticosteroids, as compared with corticosteroid monotherapy, induced faster remission of corneal inflammation and new vessels in pediatric patients with non-infectious marginal keratitis. Altogether, our findings demonstrate a pathogenic role of ocular microbiota in non-infectious inflammatory disorders leading to sight-threatening corneal neovascularization, and suggest a therapeutic potential of targeting commensal microbes in treating ocular inflammation.

*Mucosal Immunology* (2022) 15:1350–1362; <https://doi.org/10.1038/s41385-022-00555-2>

## INTRODUCTION

Over the past two decades, research has demonstrated that the microbiota inhabiting the mucosal-barrier sites of mammalian hosts is crucial for the induction, education, and function of the host immune system<sup>1,2</sup>. The microbiota can either protect their ecological niche by regulating barrier immunity or promote disease by acting as direct pathogens or adjuvants to the immune system. Importantly, the pathogenicity of a microbe or its capacity to maintain tissue homeostasis is highly dependent on the context of the given disease, host, microbe, and localization site.

Most studies thus far have focused on the composition and function of gut microbiota in both the health and disease states<sup>3</sup>. Increasing evidence indicates that gut microbiota impacts not only intestinal diseases but also diseases in tissues distant from the gut<sup>4,5</sup> such as ocular diseases<sup>6–13</sup>. Although the gastrointestinal tract is the largest reservoir of microbes in the human body, extra-intestinal tissues such as the skin, the oral cavity, the airways, and the vagina are also natural habitats of distinct microbial communities, as identified by the Human Microbiome Project (<https://www.hmpdacc.org/14–16>). Hence, it can be postulated that the extra-intestinal microbiota plays a role in the control of

tissue-specific immunity and homeostasis, as tailored to their respective niches.

The ocular surface is directly exposed to the external environment, and as such, harbors a unique microbial community containing commensal, symbiotic, and pathogenic microorganisms that is collectively referred to as the ocular surface microbiota. Characteristically, the ocular surface microbiota is remarkably lower in abundance and diversity, compared to what has been reported for other mucosal surfaces<sup>7,17–23</sup>. It is unclear whether and how the small number of ocular microbiota influences the immune response in the eye. A better understanding of the role of ocular microbiota in ocular health and disease would bring new insights into the pathogenesis of disease and chart new treatment paths.

In the present study, we investigated the effects of ocular microbiota on non-infectious corneal inflammation and angiogenesis using a mouse model of suture-induced inflammatory corneal neovascularization (NV). We also analyzed a cohort of pediatric patients with non-infectious marginal keratitis. Our data indicate that microbial stimuli may combine to drive sterile corneal inflammation and angiogenesis, suggesting a pathogenic role of

<sup>1</sup>Laboratory of Ocular Regenerative Medicine and Immunology, Biomedical Research Institute, Seoul National University Hospital, 101 Daehak-ro, Jongno-gu, Seoul 03080, Republic of Korea. <sup>2</sup>Department of Ophthalmology, Seoul National University College of Medicine, 103 Daehak-ro, Jongno-gu, Seoul 03080, Republic of Korea. <sup>3</sup>Department of Anatomy and Cell Biology, Seoul National University College of Medicine, 103 Daehak-ro, Jongno-gu, Seoul 03080, Republic of Korea. <sup>4</sup>Fight against Angiogenesis-Related Blindness (FARB) Laboratory, Biomedical Research Institute, Seoul National University Hospital, 101 Daehak-ro, Jongno-gu, Seoul 03080, Republic of Korea. <sup>5</sup>Department of Biological Sciences, Seoul National University College of Medicine, 103 Daehak-ro, Jongno-gu, Seoul 03080, Republic of Korea. <sup>6</sup>Department of Microbiology and Immunology, Seoul National University College of Medicine, 103 Daehak-ro, Jongno-gu, Seoul 03080, Republic of Korea. <sup>7</sup>These authors contributed equally: Hyun Ju Lee, Chang Ho Yoon. ✉email: jooyounoh77@gmail.com

Received: 21 November 2021 Revised: 30 July 2022 Accepted: 4 August 2022

Published online: 19 August 2022

ocular microbiota in non-infectious ocular inflammatory disorders and a therapeutic potential of targeting commensal microbes to treat ocular inflammation.

## RESULTS

### Oral antibiotics attenuate pathologic corneal NV while suppressing corneal and systemic innate immune responses

To evaluate the impact of commensal bacteria on non-infectious corneal inflammation, we used a well-established mouse model of sterile suture-induced inflammatory corneal NV<sup>24–26</sup>. Our experimental design is presented in Fig. 1a.

To deplete the commensal bacteria, we treated 8-week-old male C57BL6/N mice with a broad-spectrum oral antibiotic cocktail (ampicillin, metronidazole and vancomycin) in drinking water for 14 consecutive days (from day –7 to day 6). Seven days after treatment start (day 0), we applied 3 nylon sutures to the corneal stroma with knots unburied for induction of corneal NV. Seven days after suture injury (day 7), we performed a series of assays on the cornea, ocular draining lymph nodes (DLNs), peripheral blood, spleen and bone marrow (BM) (Fig. 1a). We picked day 7 for assays because new blood and lymphatic vessels have been shown to reach the sutures alongside a dense inflammatory cell infiltrate at 7 days after surgery in this model<sup>24–26</sup>. At baseline (before antibiotic treatment) and day 7, we also analyzed the ocular surface tissue including the conjunctiva (containing bulbar, forniceal, and tarsal conjunctiva) and eyelid margin (containing meibomian glands and eyelashes) for commensal bacteria by 16s rRNA gene sequencing as well as by conventional microbiology culture methods.

The results showed that all of the antibiotic-treated mice were negative for bacterial identification on the ocular surface by 16s rRNA gene sequencing, while all of the untreated mice were positive, indicating complete depletion of ocular surface bacteria by oral antibiotic treatment. The conventional microbiology culture on agar plates yielded no bacterial growth in either the antibiotic-treated or -untreated mice. Expectedly, suture injury to the cornea induced centripetal growth of corneal new vessels from the limbal vascular arcade, resulting in corneal opacity, as examined by slit-lamp biomicroscopy and CD31/LYVE1 immunostaining, while the normal, uninjured cornea was devoid of blood and lymphatic vessels and thus transparent (Fig. 1b). Oral antibiotic treatment significantly reduced corneal new vessel ingrowth and preserved corneal transparency (Fig. 1b, c). Moreover, corneal suturing triggered a robust inflammatory response in the cornea, as reflected by infiltration of Ly6G<sup>+</sup> neutrophils (Fig. 1d) and increased levels of activated neutrophil-derived enzyme myeloperoxidase (MPO) and pro-inflammatory and pro-angiogenic molecules IL-6, IL-1 $\beta$ , matrix metalloproteinase-9 (MMP-9), and angiopoietin-2 (Ang2)<sup>27</sup> (Fig. 1e). Oral antibiotics markedly suppressed neutrophil infiltration and decreased the levels of MPO and pro-inflammatory and pro-angiogenic factors in the cornea (Fig. 1d, e).

Further analysis for systemic immune response revealed that corneal suture injury provoked enlargement of the spleen on gross examination (Fig. 1f) and elevated the numbers of CD11b<sup>+</sup>Ly6C<sup>+</sup> and CD11b<sup>+</sup>Ly6G<sup>+</sup> myeloid cells in the spleen, BM, blood and DLNs, as measured by flow cytometry (Fig. 1g, h), indicating that a systemic innate immune response had ensued after sterile corneal injury. Notably, oral antibiotic treatment prevented splenic enlargement (Fig. 1f) and reduced the proportions of CD11b<sup>+</sup>Ly6C<sup>+</sup> cells and CD11b<sup>+</sup>Ly6G<sup>+</sup> cells in the spleen, blood, BM, and DLNs (Fig. 1g, h). On the other hand, CD4<sup>+</sup> T cells or CD4<sup>+</sup>CD25<sup>+</sup>Foxp3<sup>+</sup> regulatory T cells (Tregs) were unchanged in any of examined tissues by oral antibiotic treatment (Fig. S1).

In the aggregate, these data demonstrate that treatment of mice with oral antibiotics eradicated commensal bacteria on the ocular surface, suppressed corneal and systemic innate immune

responses, and ameliorated pathologic corneal NV induced by sterile injury.

### Topical fluoroquinolone recapitulates effects of oral antibiotics

To eliminate the ocular microbiota more specifically, we treated 8-week-old male C57BL6/N mice with topical fluoroquinolone eye drops (moxifloxacin; Vigamox<sup>®</sup>, Alcon, Geneva, Switzerland) QID for 14 consecutive days (from day –7 to day 6). At day 0, we applied suture injuries to the cornea, and at day 7, carried out assays. The experimental scheme is depicted in Fig. 2a.

As expected, no bacteria were identified on the ocular surfaces of the topical antibiotic-treated mice by 16s rRNA sequencing and microbiology culture. Biomicroscopic observation and CD31/LYVE1 immunostaining of the cornea revealed that topical fluoroquinolone was as effective as systemic antibiotics in suppressing corneal NV and subsequently preventing corneal opacity against injury (Fig. 2b–d). A real-time RT-PCR assay showed that the corneal levels of CD31 and angiogenic growth factors VEGF-A and -C were significantly lower in the topical fluoroquinolone-treated mice relative to the untreated mice (Fig. 2e), which correlated with the downregulation of pathologic corneal angiogenesis by the topical antibiotics. Moreover, topical treatment with fluoroquinolone significantly suppressed neutrophil infiltration (Fig. 2d) and reduced the levels of pro-inflammatory and pro-angiogenic factors TNF- $\alpha$ , IL-1 $\beta$ , IL-6, MMP-9, and Ang2 in the cornea (Fig. 2f).

Similarly to its effects on local immune response, topical fluoroquinolone repressed systemic immune response. The splenic enlargement induced by corneal injury was inhibited by topical fluoroquinolone treatment (Fig. 2g). The proportions of CD11b<sup>+</sup>Ly6C<sup>+</sup> cells and CD11b<sup>+</sup>Ly6G<sup>+</sup> cells in the spleen, blood and DLNs, moreover, were significantly lowered by the topical fluoroquinolone, as analyzed by flow cytometry (Fig. 2h, i). Topical fluoroquinolone did not reduce CD11b<sup>+</sup>Ly6C<sup>+</sup> or CD11b<sup>+</sup>Ly6G<sup>+</sup> cells in BM (data not shown), unlike the oral antibiotics, and neither did it affect CD4<sup>+</sup>CD25<sup>+</sup>Foxp3<sup>+</sup> Tregs in DLNs, blood, spleen, or BM (Fig. S2).

Additionally, we assayed the influence of topical antibiotics on the gut microbiota (Fig. S3A). Topical fluoroquinolone reduced the abundance of phylum *Proteobacteria* (from 1.8% to 0.02%) (Fig. S3B) and the richness of microbiota (Fig. S3C), but it did not affect the abundance of the predominant bacterial phyla and diversity (Fig. S3B, D, E). Moreover, these effects were slight relative to the disruption of gut microbiota by oral broad-spectrum antibiotic cocktail<sup>28</sup>.

Altogether, the results suggest that topical antibiotics removed ocular bacteria and effectively repressed the ocular and systemic innate immune responses induced by sterile injury to the cornea, thereby attenuating pathologic corneal NV.

### Ocular surface microbiota is unaltered by injury

The normal ocular surface microbiome is paucibacterial and contains core bacteria including commensal, environmental, and opportunistic pathogenic species<sup>7,17–23</sup>. Since we had observed the therapeutic effects of antibiotic-induced depletion of ocular microbiota on sterile inflammatory corneal NV (Figs. 1 and 2), we next examined whether sterile suture injury to the cornea might cause alterations in the ocular surface microbiota in 8-week-old C57BL6/N mice (Fig. 3a).

A survey of the ocular surface microbiota by 16S rRNA sequencing revealed that they were composed mainly of *Actinobacteria* (63.4%), *Firmicutes* (18.9%), and *Proteobacteria* (13.9%) at the phylum level, accounting for >96% of all sequences (Fig. 3b). The average number of distinct operational taxonomic units (OTUs) was 130 in normal eyes without injury (Fig. 3c). Corneal injury did not induce significant changes in either the number of OTUs or the relative abundance of major bacterial taxa

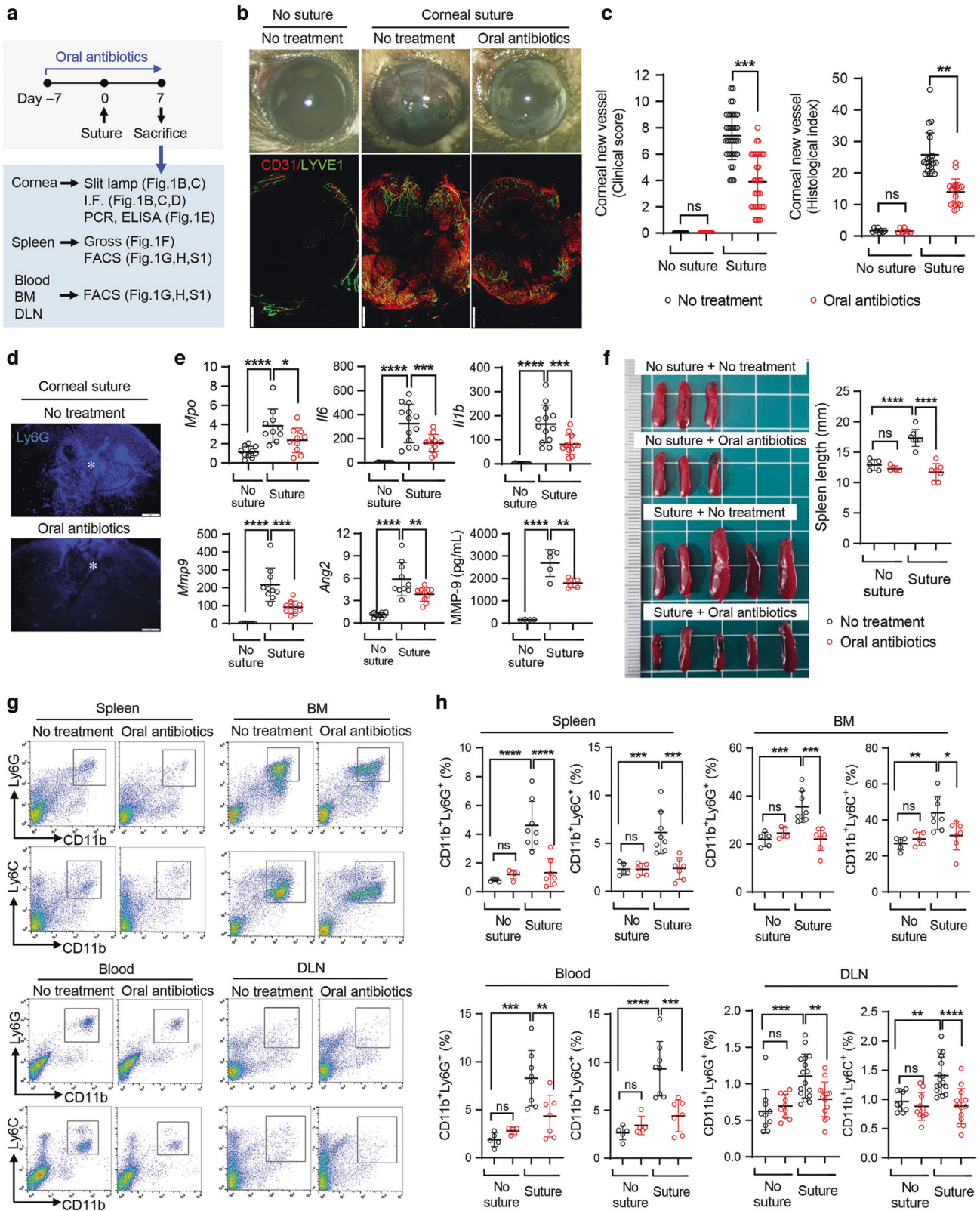


(Fig. 3b, c). Furthermore, there were no significant differences in the richness or diversity of ocular surface microbiota between uninjured and injured eyes, as determined by  $\alpha$ -diversity (Chao1, Shannon-Weaver, and Simpson indices) and  $\beta$ -diversity (Fig. 3c–e). These data indicated that the suture injury to the cornea had no influence on the ocular surface microbial composition.

**Fluoroquinolone does not impair vascular endothelial cells**

Previous studies have reported that fluoroquinolones can cause immediate toxicity to vascular cells<sup>29</sup> and affect pro-inflammatory activation of monocytes/macrophages<sup>30,31</sup>. Hence, to rule out the possibility that the therapeutic effects of fluoroquinolone on corneal NV and inflammation (Fig. 2) are due to its action on

**Fig. 1 Oral antibiotics ameliorate corneal NV by suppressing corneal and systemic immune responses.** **a** Experimental protocol. Eight-week-old C57BL6/N mice were given an oral antibiotic cocktail (ampicillin, metronidazole and vancomycin) in drinking water for 14 days (from day -7 to day 6). On day 0, the mice were subjected to three sterile suture injuries per cornea for induction of inflammatory angiogenesis. On day 7, assays were performed on the cornea, spleen, peripheral blood, bone marrow (BM) and ocular draining cervical lymph nodes (DLN). **b** Representative corneal photographs and microphotographs of whole-corneal mounts with CD31/LYVE1 immunostaining. Scale bar: 500  $\mu\text{m}$ . **c** Clinical scoring of corneal new vessels ( $n = 16$  eyes for no suture/no treatment group;  $n = 16$  eyes for no suture/oral antibiotics group;  $n = 38$  eyes for suture/no treatment group;  $n = 36$  eyes for suture/oral antibiotics group) and quantification of CD31-stained area in corneal flat mounts. **d** Representative microphotographs of whole-corneal mounts with Ly6G immunostaining. Scale bar: 200  $\mu\text{m}$ . The asterisk marks the corneal suture location. **e** mRNA levels of activated neutrophil marker (myeloperoxidase, MPO), pro-inflammatory cytokines (IL-6 and IL-1 $\beta$ ) and pro-angiogenic factors (MMP-9 and Ang2) in the cornea, as analyzed by real-time RT-PCR. Values are shown relative to those in C57BL6/N control corneas that had not received injury or treatment. Protein level of MMP-9 in the cornea as analyzed by ELISA. **f** Gross photographs of spleen and measurement of spleen size in length. **g** Representative flow cytometry cytograms of CD11b<sup>+</sup>Ly6G<sup>+</sup> and CD11b<sup>+</sup>Ly6C<sup>+</sup> cells in spleen, BM, blood and DLN. **h** Quantification of CD11b<sup>+</sup>Ly6G<sup>+</sup> and CD11b<sup>+</sup>Ly6C<sup>+</sup> cells as measured by flow cytometry in spleen, BM, blood, and DLN. The numbers indicate % of total cells. Mean values  $\pm$  SD are shown in graphs, where each circle depicts the data from an individual mouse. Data are pooled from 2 to 4 independent experiments. \* $p < 0.05$ , \*\* $p < 0.01$ , \*\*\* $p < 0.001$ , \*\*\*\* $p < 0.0001$ , ns: not significant, analyzed either by one-way ANOVA with Tukey's multiple-comparison test (**e**, **f**, **h**) or Kruskal-Wallis test with Dunn's multiple-comparisons test (**c**).

vessels and immune cells, we went on to investigate the direct effects of fluoroquinolone in cultures of vascular endothelial cells, monocytes/macrophages, and splenocytes.

Angiogenesis processes indicate new vessel formation from the existing vessels and include tube formation, migration, and proliferation of vascular endothelial cells<sup>32</sup>. To figure out whether fluoroquinolone by itself affects angiogenesis processes, we treated human umbilical vein endothelial cells (HUVECs) with various concentrations of moxifloxacin (0–5000  $\mu\text{g}/\text{mL}$ ), and performed tube formation, migration and cell viability assays (Fig. 4a). The responses of HUVECs in culture have been shown similar to those of corneal new vessels in vivo<sup>33–37</sup>. In the tube formation assay, moxifloxacin did not reduce the tube-formation potential of the HUVECs at concentrations between 1 and 500  $\mu\text{g}/\text{mL}$  (Fig. 4b, c). Likewise, in the cell migration assay, the HUVECs retained their ability to migrate under moxifloxacin treatment (1–500  $\mu\text{g}/\text{mL}$ ) (Fig. 4d, e). Furthermore, moxifloxacin (1–100  $\mu\text{g}/\text{mL}$ ) did not change the cell viability of the HUVECs (Fig. 4f).

These data indicate that the inhibitory effects of fluoroquinolone on corneal NV might not be associated with its direct effects on vascular endothelial cells and subsequent angiogenesis processes.

### Fluoroquinolone does not affect survival or phenotype of immune cells

In a parallel experiment, we treated THP-1-differentiated human macrophages or mouse splenocytes with a broad range of concentrations of moxifloxacin (0–1000  $\mu\text{g}/\text{mL}$ ) in the presence or absence of 100 or 1000 ng/mL lipopolysaccharide (LPS) stimulation for 18 h, and then conducted a series of assays for evaluation of cell apoptosis, inflammatory cytokine production, surface marker expression, and phagocytic activity (Fig. 5a).

Moxifloxacin (5–100  $\mu\text{g}/\text{mL}$ ) did not increase the number of annexin (ANX)<sup>+</sup>propidium iodide (PI)<sup>+</sup> cells or ANX<sup>+</sup>PI<sup>-</sup> cells in the human macrophages or mouse splenocytes (Figs. 5b, c, S4). Furthermore, clinically-relevant concentrations of moxifloxacin (5–10  $\mu\text{g}/\text{mL}$ ) did not alter the production of pro-inflammatory cytokines TNF- $\alpha$ , IL-1 $\beta$  and IL-6, though high concentrations of moxifloxacin (100  $\mu\text{g}/\text{mL}$  or higher) decreased the pro-inflammatory cytokine production (Fig. 5d). Moxifloxacin (5–500  $\mu\text{g}/\text{mL}$ ) did not induce the secretion of anti-inflammatory molecules IL-10, prostaglandin E2 (PGE2), amphiregulin (AREG), active TGF- $\beta$ 1 or TGF- $\beta$ 2 in the cells (Fig. S5). Similarly, moxifloxacin (up to 100–500  $\mu\text{g}/\text{mL}$ ) did not change the levels of major histocompatibility complex (MHC) class II molecule or co-stimulatory molecule CD80 on the cell surface (Fig. 5e, f). Moreover, moxifloxacin, at all of the tested concentrations, had no effect on the phagocytic activity of macrophages, as assessed by fluorescent BioParticle uptake assay (Fig. 5g).

Taken together, the data suggest that moxifloxacin, at therapeutic concentrations, did not directly influence the viability or functions of vascular endothelial cells or immune cells.

### Topical antibiotic treatment induces faster remission of non-infectious keratitis in patients

To verify the beneficial effects of antibiotics in a clinical setting, we surveyed a cohort of pediatric patients (aged 15 years and younger) with marginal keratitis, a non-infectious disease characterized by recurrence of corneal inflammation and NV that can result in vision-threatening corneal opacification.

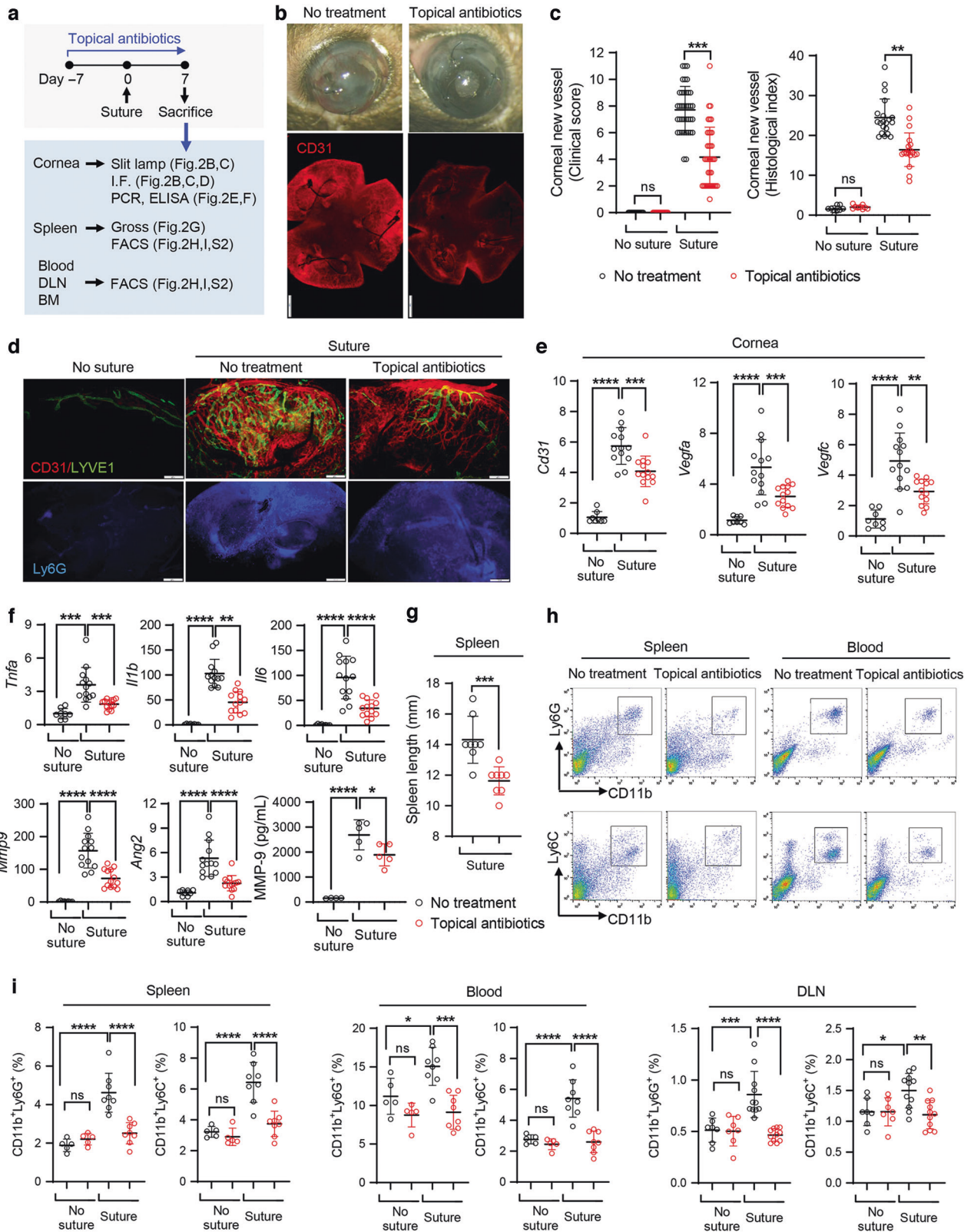
Out of a total of 117 patients, 20 were included in the study after being matched for patient age, gender, and disease severity at disease onset. Amongst them, 15 patients were treated with a combination of topical antibiotics and corticosteroids, while 5 were treated only with topical corticosteroids. We compared the treatment outcomes between the two groups. The baseline demographics, clinical characteristics, and treatment outcomes are summarized in Table 1.

Overall, complete remission was achieved in 19 of 20 patients (95%): in 4 of 5 patients (80%) with topical steroid monotherapy and in 15 of 15 patients (100%) with topical antibiotic/corticosteroid combination therapy (Table 1, Fig. 6a–l). Analysis by Kaplan-Meier survival curves demonstrated that the median time from treatment start to disease remission (i.e., complete resolution of corneal infiltrates and regression of new vessels) was significantly shorter in the patients treated with the antibiotic/corticosteroid combination than in those treated with corticosteroid alone (2 weeks vs. 4.5 weeks,  $p = 0.034$ ) (Fig. 6m). Consistently with these data, the mean time to disease remission was significantly faster in the group treated with the antibiotic/corticosteroid combination therapy than in the group treated with corticosteroid monotherapy ( $2.0 \pm 0.9$  week vs.  $5.5 \pm 3.7$  weeks,  $p = 0.049$ ) (Fig. 6n, Table 1). Visual acuity improved in all patients by either treatment, from logMAR  $0.17 \pm 0.19$  before treatment to logMAR  $0.05 \pm 0.09$  after treatment ( $p = 0.002$ ) (Table 1).

### DISCUSSION

In this study, elimination of ocular microbiota by oral or topical antibiotics suppressed the activation of systemic and ocular immune systems in response to sterile corneal injury, and attenuated pathologic corneal NV in mice and humans. These findings suggest that the ocular surface microbiota can collectively act as an adjuvant in the sterile-injury setting, providing innate danger signals that trigger and drive the host immune response for pathogenicity.

The ocular surface is in constant contact with the external environment, and as such, is well-equipped with the “mucosal



firewall” to segregate and defend against potentially pathogenic microbes. The ocular surface is continuously cleared by lid blinking and tear secretion. The tear film contains a multitude of antimicrobial peptides including lysozymes, immunoglobulins, lactoferrin, and defensins<sup>38</sup>. Moreover, the stratified corneal

epithelium (and, to a lesser extent, the conjunctival epithelium) featuring tight junctions and desmosomes forms the primary barrier against microbial translocation. The corneal and conjunctival epithelial barriers are additionally reinforced by the glycocalyx system involving a soluble mucin MUC5AC secreted

**Fig. 2 Topical fluoroquinolone attenuates corneal NV by repressing corneal and systemic immune responses.** **a** Experimental protocol. Topical moxifloxacin eye drops (Vigamox<sup>®</sup>) were instilled to the ocular surface of 8-week-old C57BL6/N mice QID for 14 days (from day -7 to day 6). On day 0, three sterile sutures were applied to the cornea for induction of inflammatory corneal angiogenesis. On day 7, assays were conducted in the cornea, spleen, peripheral blood, draining cervical lymph nodes (DLN) and bone marrow (BM). **b** Representative corneal photographs and microphotographs of corneal flat mounts with CD31 immunostaining. Scale bar: 500  $\mu$ m. **c** Clinical scoring of corneal new vessels ( $n = 16$  eyes for no suture/no treatment group;  $n = 16$  eyes for no suture/topical antibiotic group;  $n = 38$  eyes for suture/no treatment group;  $n = 38$  eyes for suture/topical antibiotic group) and measurement of CD31-stained areas in corneal flat mounts. **d** Representative microphotographs of corneal flat mounts with CD31/LYVE1 or Ly6G staining. Scale bar: 200  $\mu$ m. **e** Real-time RT-PCR for endothelial marker (CD31) and vascular growth factors (VEGF-A and -C) in cornea. The mRNA levels are presented as fold changes relative to the levels in normal corneas without injury or treatment. **f** Real-time RT-PCR for pro-inflammatory cytokines (TNF- $\alpha$ , IL-1 $\beta$ , and IL-6) and pro-angiogenic factors (MMP-9 and Ang2) in cornea. The mRNA levels are shown relative to those in normal corneas that had not received injury or treatment. ELISA for MMP-9 protein level in the cornea. **g** Measurement of splenic size on gross examination. **h** Representative flow cytometry cytograms of CD11b<sup>+</sup>Ly6G<sup>+</sup> and CD11b<sup>+</sup>Ly6C<sup>+</sup> cells in spleen and peripheral blood. **i** Quantification of CD11b<sup>+</sup>Ly6G<sup>+</sup> and CD11b<sup>+</sup>Ly6C<sup>+</sup> cells as analyzed by flow cytometry in spleen, blood and DLN. The numbers indicate % of total cells. Mean values  $\pm$  SD are shown, and a circle depicts the data from a single animal. Data are pooled from two to four independent experiments. \* $p < 0.05$ , \*\* $p < 0.01$ , \*\*\* $p < 0.001$ , \*\*\*\* $p < 0.0001$ , ns: not significant, as analyzed by one-way ANOVA with Tukey's multiple-comparison test (E, *Tnfa*, *Il6*, *Mmp9* and *Ang2* in **f**, **i**), Kruskal–Wallis test with Dunn's multiple-comparisons test (C, *Il1b* in **f**), or Student's *t* test test (**g**).

by conjunctival goblet cells along with transmembrane mucins MUC1, MUC4, and MUC16 produced by the conjunctival and corneal epithelia<sup>39–41</sup>. Furthermore, both the innate and adaptive immune systems are involved in eliminating translocating microbes and limiting inflammation<sup>42,43</sup>. Hence, the healthy ocular surface has a remarkably low number of microorganisms and few microbial species<sup>7,17–23</sup>, as we observed in the present study. Despite this low abundance and lack of species diversity, our findings suggest that the ocular surface microbiota has the capacity to facilitate corneal inflammation and angiogenesis upon sterile injury, and that the ocular surface microbial stimuli play an important role in the induction and propagation of danger signals in the early phase of the amplification loop of inflammation, subsequently leading to the activation of the systemic immune system.

Most studies to date have focused on exploring the effects of gut microbiota, the largest density of commensals, on ocular health and disease, demonstrating their profound role in the pathogenesis of various ocular diseases. Notably, the capacity of the microbiota to trigger or prevent disease is highly dependent on the context. An elegant study by Horai, Zárate-Bladés et al.<sup>9</sup> demonstrated that depletion of commensal microbiota in mice by oral antibiotics or under the germ-free condition decreased the severity of experimental autoimmune uveitis (EAU), an intraocular autoimmune disease. Mechanistically, the commensal microbes activated retinal-specific Th17 cells in the gut through interaction with autoreactive T cell receptors. Similar studies have confirmed that gut-microbiota alterations in oral-antibiotic-treated mice or germ-free mice ameliorated EAU through reduction of effector T cells and expansion of Foxp3<sup>+</sup> Tregs<sup>10,44</sup>. As for corneal disease, it was reported that depletion of gut microbiota by broad-spectrum oral antibiotics significantly decreased corneal angiogenesis and inflammation in a mouse model of herpes simplex virus keratitis<sup>45</sup>. Also, a recent study by Sato et al. showed that oral antibiotic administration alleviated ocular graft-versus-host disease (GVHD) manifestations in the cornea by increasing Tregs and suppressing Th17 cells and IL-6-producing macrophages in a chronic GVHD mouse model<sup>46</sup>. On the other hand, there are many reports demonstrating the protective role of gut microbiota in various ocular disease models including choroidal NV<sup>47</sup>, dry eye disease<sup>6,8</sup>, infectious keratitis<sup>48</sup>, corneal nerve regeneration<sup>11</sup>, and corneal development<sup>12</sup>. In our study, topical antibiotic treatment to the eye was as effective as oral broad-spectrum antibiotics in reducing corneal NV and inflammation upon sterile injury, suggesting the important role of ocular microbiota in the induction of inflammatory corneal angiogenesis. However, given the potential effect of topical fluoroquinolone on the gut microbiota (e.g., reduction of its richness), the possibility could not be ruled out that the beneficial effects of topical or oral antibiotics might be attributable to changes in the gut microbiota as well as depletion of the ocular microbiota.

These recent findings that the gut and ocular microbiota are involved in pathogenic and homeostatic mechanisms open avenues for new strategies for the treatment or prevention of disease through modulation of the microbiota. Importantly, the impact of commensal microbiota is double-edged and highly depends on the specific disease context. Therefore, identification of the causative microorganisms and their products/metabolites that are primarily responsible for pathogenicity or maintenance of homeostasis in a specific disease would be crucial for development of novel therapies targeting the microbiota. In our study, generalized suppression of commensal microbes by antibiotics was beneficial for treating non-infectious corneal inflammatory NV in mice and humans, suggesting that the normal microbiome at the ocular surface contributes to pathogenesis under pathologic conditions. On the other hand, many studies have reported detrimental effects of systemic and ophthalmic antibiotic therapies on the ocular surface: specifically, alteration of the ocular surface microbiota and potential contribution, thereby, to the opportunistic invasion of pathogenic species and antibiotic resistance in microbes<sup>21,48–55</sup>. Hence, a further investigative step should be to identify the causative bacteria within the normal microbiome and excise those responsible for neovascular inflammation in the cornea. Certainly, selective treatment of a specific pathogenic species and pathway would offer a more effective and safe therapy for non-infectious corneal inflammatory disorders leading to vision-threatening corneal NV.

In conclusion, our study strengthens the notion that bacterial stimuli are involved in driving sterile-injury-induced inflammation, and identifies a pathogenic role of ocular microbiota in non-infectious inflammatory corneal NV. These findings have clinical implications not only for the use of antibiotics for ocular surface disease but also for the development of novel treatments targeting pathogenic ocular microbiota.

## METHODS

### Animal and animal model

Animal experiments were performed in accordance with the ARVO statement on the use of animals in ophthalmic and vision research. The experimental protocols were approved by the Institutional Animal Care and Use Committee of Seoul National University Hospital Biomedical Research Institute (Seoul, Korea) (IACUC No. 19-0069). Blinding and randomization were used during animal allocation, the conduct of experiments, the outcome assessment and the data analysis.

Eight-week-old male C57BL6/N mice were purchased from KOATECH (Pyeongtaek, Korea) and housed in a specific pathogen-free environment. The mice were freely fed a normal diet of laboratory rodent chow (38,057, Cargill Agri Purina, Seongnam, Korea) and water ad libitum.

For induction of inflammatory corneal NV, mice were anesthetized by intraperitoneal injection of zolazepam-tiletamine (Zoletil<sup>®</sup>, Virbac, Carros,

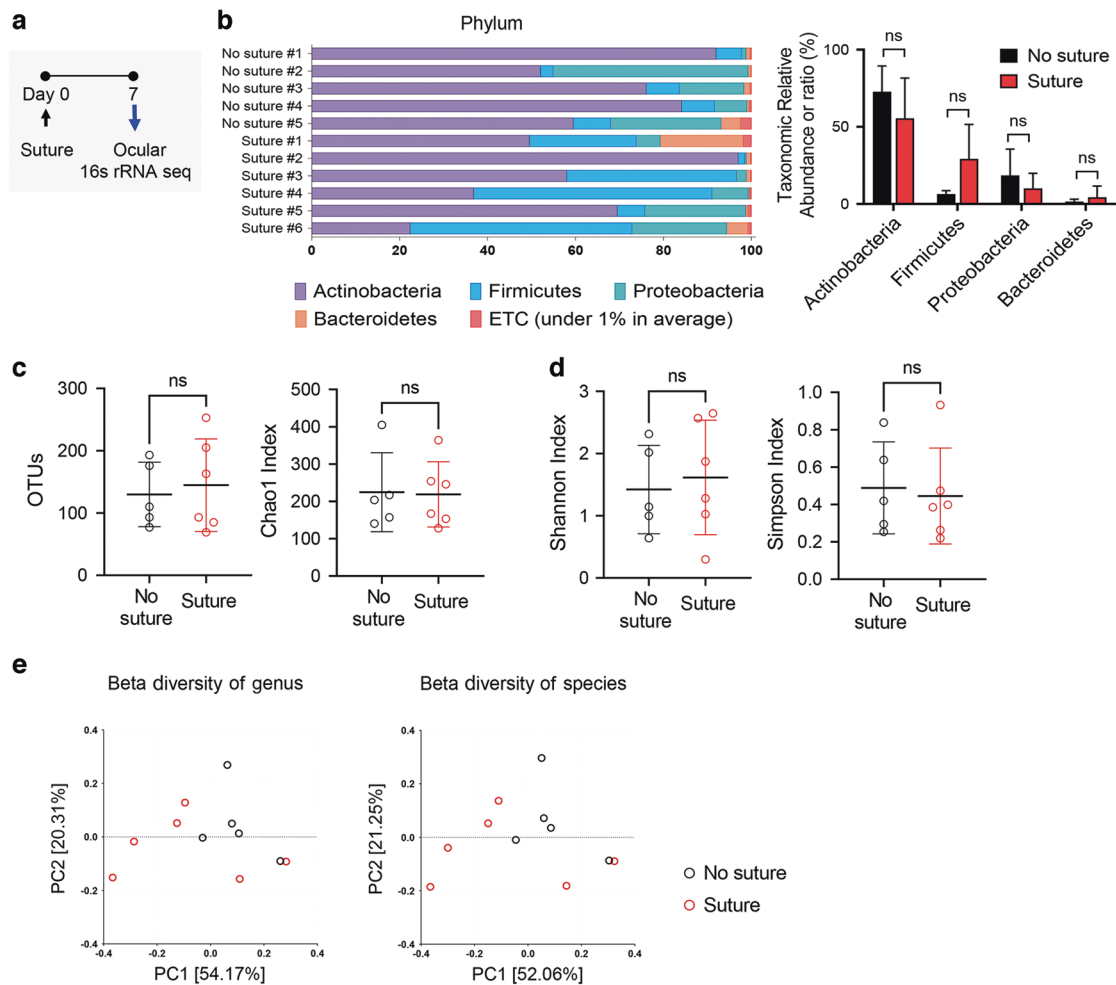


**Fig. 3 Suture injury does not induce substantial changes in ocular surface microbiome.** **a** Experimental protocol. Eight-week-old C57BL6/N mice were subjected to three sterile suture injuries per cornea for induction of inflammatory angiogenesis. Seven days later, the ocular surface microbiota analysis was performed. **b** Relative abundance at phylum level. The phyla with more than 1% abundance in at least one group were analyzed. No significant differences were found between the groups. **c** Observed operational taxonomic unit (OTU) count and Chao1 index. **d** Shannon-Weaver and Simpson indices. **e**  $\beta$ -diversity of genus and species, as measured by UniFrac principal coordinates analysis (PCoA), showed no significant differences between the groups. Mean values  $\pm$  SD are shown in graphs, where each circle depicts the data from an individual mouse. ns: not significant by Mann-Whitney *U* test.

France) and topical administration of 0.5% proparacaine hydrochloride ophthalmic solution (Hanmi Pharm Co., Ltd., Seoul, Korea). Three 10–0 nylon sutures were placed in the corneal stroma 2 mm from the pupil center and 120° apart from each other, and the knots were left unburied<sup>24,26</sup>.

#### Antibiotic treatment and depletion of ocular surface microbiota

For oral antibiotic treatment, mice were treated with a combination of broad-spectrum antibiotics dissolved in drinking water: 1 mg/mL ampicillin (Sigma-Aldrich, St. Louis, MO), 1 mg/mL metronidazole (Sigma-Aldrich) and 0.5 mg/mL vancomycin (MP Biomedicals, Irvine, CA).

For topical antibiotic treatment, moxifloxacin eye drops (Vigamox®, Alcon, Geneva, Switzerland) were topically administered QID to the ocular surfaces of the mice. The eyes were kept open for 30 s after instillation of eye drops to prevent blinking and ensure absorption of the drops.

Complete depletion of the ocular surface microbiota was verified by two methods of bacteriologic analysis: conventional bacterial culture and 16S rRNA gene amplification/sequencing.

#### Bacterial culture

The mouse conjunctivae including the superior and inferior fornices were swabbed and plated on universal and differential media including blood agar and MacConkey agar plates in the Microbiology Core Facility at the Seoul National University Hospital Biomedical Research Institute (Seoul, Korea).

#### DNA extraction from mouse eyes, 16S rRNA gene amplification/sequencing

For ocular surface microbiota analysis, the whole conjunctiva (including bulbar, fornical and tarsal conjunctivae) and eyelid margin (including meibomian glands and eyelashes) were excised. For the gut microbiota analysis, feces were collected. All of the collected tissues were stored at  $-80^{\circ}\text{C}$  and transferred to Chunlab (Seoul, Korea) for microbiota analysis<sup>56</sup>. Total DNA extraction was performed using the FastDNA® SPIN Kit for Soil (MP Biomedicals) in accordance with the manufacturer's instructions. PCR amplification was carried out using extracted DNA and bacterial PCR primers 341F (5'-TCGTCGGCAGCGTC-AGATGTGATAAGA GACAG-CCTACGGGNGGCWGCAG-3'; underlining sequence indicates the target region primer) and 805R (5'-GTCTCTGGGCTCGG-AGATGTGATAAGAGACAG-GACTACHVGGGTATCTAATCC-3') targeting the V3-V4 regions of 16S rRNA. The reaction conditions for the first PCR amplification were as follows: 3 min of initial denaturation at 95 °C, 25 cycles of 30 s denaturation at 95 °C, 30 s primer annealing at 55 °C, 30 s elongation at 72 °C, and final extension at 72 °C for 5 min. The second PCR amplification was carried out using i5 forward primer (5'-AATG ATACGGCACCACCGAGATCTACAC-XXXXXXXX-TCGTCGGCAGCGTC-3'; X indicates the barcode region) and i7 reverse primer (5'-CAAGCAGAAGACGGCATAACGAGAT-XXXXXXXX-GTCTCTGGGCTCGG-3') for attachment of the Illumina Nextera barcode. The second amplification conditions were the same as those described for the first reaction, except that only eight amplification cycles were performed. Amplification was confirmed using

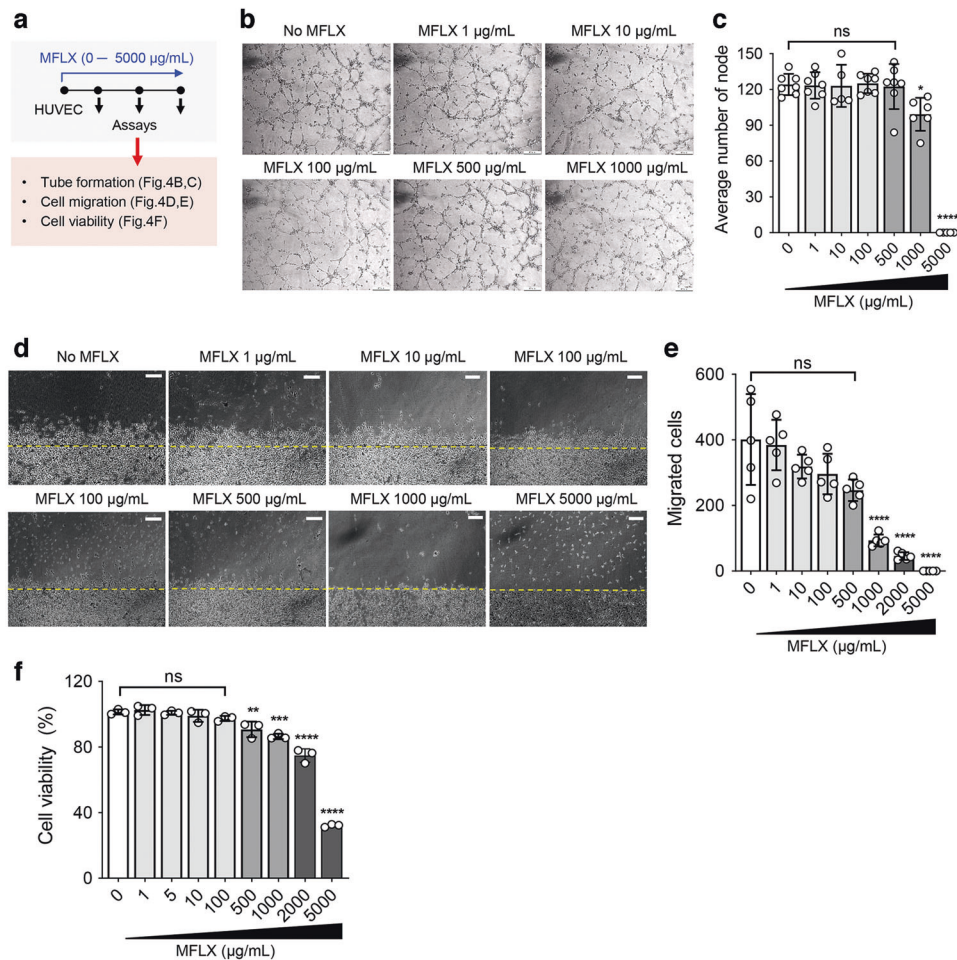


**Fig. 4** Therapeutic concentrations of moxifloxacin do not inhibit angiogenesis processes of vascular endothelial cells. **a** Experimental scheme. Human umbilical vein endothelial cells (HUVECs) were treated with moxifloxacin (MFLX) (0–5000 µg/mL). 12 h later, assays were performed for evaluation of tube formation, cell migration, and cell viability. **b** Representative photographs of HUVECs in tube formation assay. **c** Quantification of tube formation of HUVECs. The numbers indicate the nodes of vascular tubes in random ×100 microscopic fields. **d** Representative photographs of HUVECs in migration assay. The yellow dotted lines are the reference lines. Scale bar: 50 µm. **e** Quantification of cell migration of HUVECs. The numbers indicate the numbers of cells beyond the reference lines. **f** Quantification of cell viability of HUVECs, as assessed by EZ-CYTOX cell viability assay. Values are shown relative to those in the control HUVECs, which had not been treated with moxifloxacin. Mean values ± SD are shown, and a circle depicts the data from a single well or plate. \* $p < 0.05$ , \*\* $p < 0.01$ , \*\*\* $p < 0.001$ , \*\*\*\* $p < 0.0001$ , ns: not significant, as analyzed by one-way ANOVA with Tukey's multiple-comparison test.

gel electrophoresis on 1% agarose gels and visualized on a Gel Doc system (BioRad, Hercules, CA). The product size and quality were evaluated on a Bioanalyzer 2100 (Agilent, Palo Alto, CA) using a DNA 7500 chip. Mixed amplicons were pooled, and sequencing was performed at Chunlab using an Illumina MiSeq Sequencing system (Illumina, San Diego, CA) according to the manufacturer's instructions. The EzBioCloud database (<http://ezbiocloud.net>), a bioinformatics cloud platform of Chunlab, was used for taxonomic classification after chimera checking. UCHIME and the non-chimeric 16S rRNA database from EzBioCloud were used to detect chimeras on reads containing a lower-than 97% best-hit similarity rate. The dataset was normalized to the lowest number of read counts (4388 reads for ocular surface tissue and 48,810 reads for feces) for further analysis.

#### Microbial community analysis

Both  $\alpha$ -diversity and  $\beta$ -diversity analyses were carried out using EzBioCloud. The observed OTUs, Chao1 and Shannon-Weaver were used as the  $\alpha$ -diversity metrics, and generalized UniFrac was employed as the  $\beta$ -diversity measure. Principal Coordinates Analysis was performed to visualize differences in the samples at the genus and species levels. Compositional abundance differences from each sample were identified by Kruskal-Wallis test. Taxa present in greater than 1% abundance in at least one group were included in the analysis.

#### Immunostaining of corneal flat mounts

For CD31, LYVE1, and Ly6G immunostaining of whole-corneal flat mounts, the excised corneas were rinsed in phosphate-buffered solution (PBS) and fixed in acetone/methanol (1:1) at room temperature (RT) for 10 min. After 2% bovine serum albumin blocking at RT for 1 h, the tissues were incubated overnight at 4 °C with anti-CD31 (1:20) (BD Pharmingen, San Diego, CA), anti-LYVE1 (1:100) (AngioBio, San Diego, CA), and BV421-conjugated anti-Ly6G (1:100) (BD Horizon, San Jose, CA), and then with goat anti-rat IgG-Cy3 (1:200) (Invitrogen, Waltham, MA) and goat anti-rabbit IgG-FITC (1:500) (Invitrogen) at RT for 3 h. The stained corneas were transferred onto slides, divided into four quadrants, flat-mounted, and examined under fluorescence confocal microscopy (Nikon, Tokyo, Japan).

#### Corneal NV quantification

Corneal NV was quantified both by clinical scoring and measurement of the CD31-stained area. For clinical scoring, the corneas were observed in vivo under slit-lamp biomicroscopy and photographed with a camera mounted on a surgical operating microscope. The extent of corneal NV was scored on a scale of 0–3 for each quadrant by two independent observers (J.Y.O. and H.J.K.) in a blinded manner using the standardized scale system (scale 0: no new vessels; scale 1: new vessels at the corneal limbus; scale 2: new vessels spanning the limbus and approaching the corneal center; scale 3: new vessels spanning the center)<sup>26,57</sup>. Scores for each quadrant were summed to



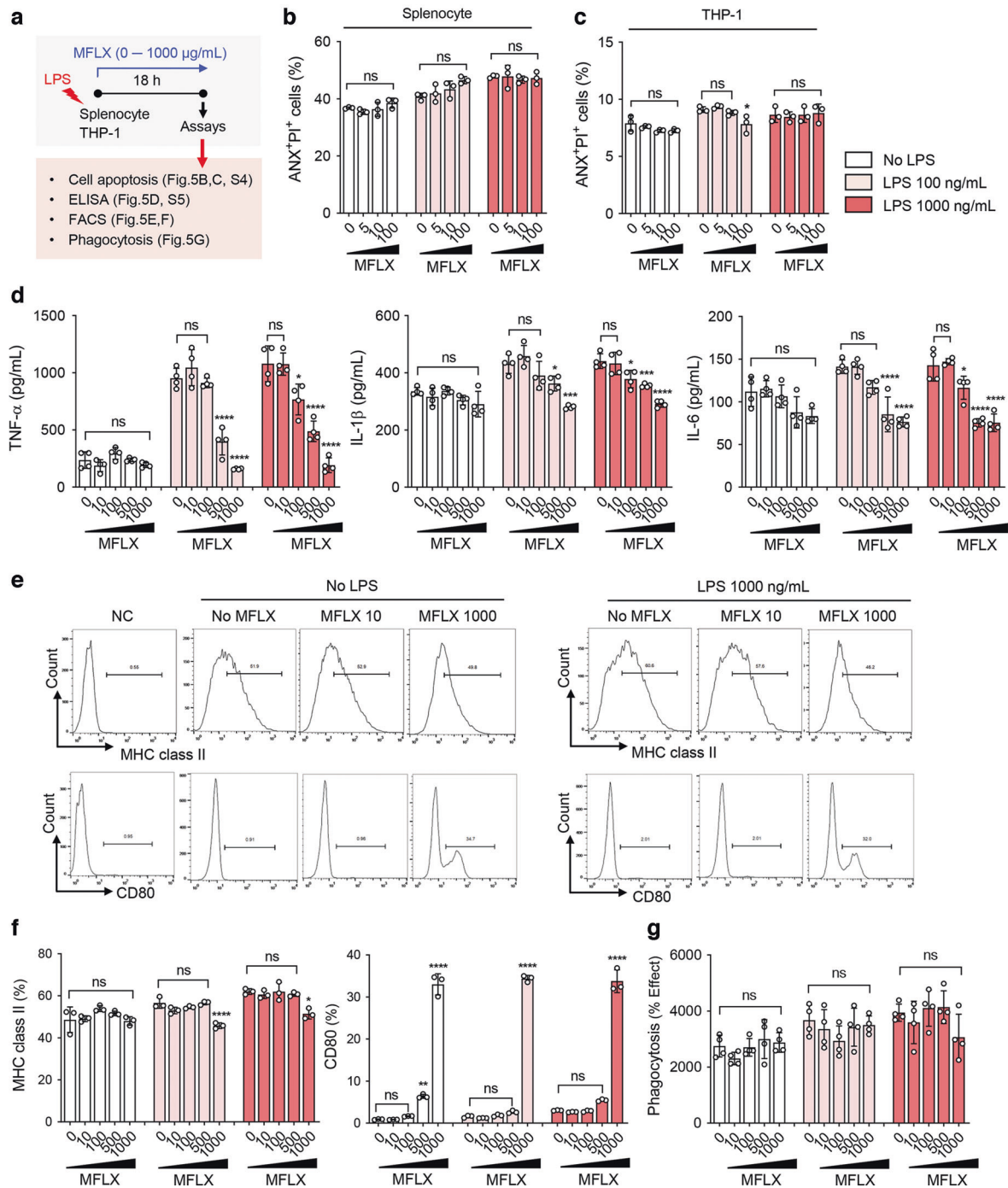


**Fig. 5** Therapeutic concentrations of moxifloxacin have no effect on survival, inflammatory phenotype, or phagocytic activity of immune cells. **a** Experimental scheme. C57BL6/N splenocytes, or THP-1-differentiated human macrophages were treated with moxifloxacin (MFLX) (0–1000 µg/mL) under lipopolysaccharide (LPS) stimulation (100 or 1000 ng/mL). 18 h later, assays were performed for evaluation of cell apoptosis, inflammatory activation, surface marker expression and phagocytic activity. **b** Quantitative flow cytometry results for annexin (ANX)<sup>+</sup>propidium iodide (PI)<sup>+</sup> cells in mouse splenocytes. **c** Quantitative flow cytometry results for ANX<sup>+</sup>PI<sup>+</sup> cells in THP-1-differentiated human macrophages. **d** ELISA for secreted levels of pro-inflammatory cytokines (TNF-α, IL-1β and IL-6) in splenocytes. **e** Representative flow cytometry histograms of major histocompatibility complex (MHC) class II and CD80 in THP-1-differentiated macrophages. **f** Quantification of MHC class II and CD80 in THP-1-differentiated macrophages. The numbers indicate the proportion of MHC class II- or CD80-expressing cells to the total cells. **g** BioParticle uptake assay for analysis of phagocytic activity in THP-1-differentiated macrophages. Shown is the % effect, which is the cells' relative phagocytic response to the phagocytosis effector agent. The data are presented in mean values ± SD, where each circle depicts data from one biological sample. \**p* < 0.05, \*\**p* < 0.01, \*\*\**p* < 0.001, \*\*\*\**p* < 0.0001, ns: not significant by one-way ANOVA with Tukey's multiple-comparison test. Asterisks indicate the values relative to no MFLX group.

**Table 1.** Demographics, disease characteristics and treatment outcomes of non-infectious marginal keratitis patients.

	Total	Topical steroid only	Topical antibiotics + steroid	p value
No. of patients	20	5	15	
Age of onset (years)	9.8 ± 2.8	9.2 ± 3.1	9.8 ± 2.8	>0.999 <sup>b</sup>
Sex (male:female)	4:16	1:4	3:12	>0.999 <sup>c</sup>
Corneal epithelial defect (Oxford grading score)	2.1 ± 1.0	2.8 ± 1.3	1.9 ± 0.8	0.430 <sup>b</sup>
Complete remission (%)	19 (95%)	4 (80%)	15 (100%)	0.250 <sup>c</sup>
Time to resolution (weeks) <sup>a</sup>	2.7 ± 2.4	5.5 ± 3.7	2.0 ± 0.9	0.049 <sup>b</sup>
Follow-up period (weeks)	93.0 ± 81.9	86.2 ± 114.1	93.3 ± 67.3	0.456 <sup>b</sup>
BCVA at initial visit (logMAR)	0.17 ± 0.19	0.20 ± 0.31	0.15 ± 0.13	0.850 <sup>b</sup>
BCVA at last visit (logMAR)	0.05 ± 0.09	0.05 ± 0.16	0.05 ± 0.05	0.514 <sup>b</sup>
P value of BCVA (initial vs last visit) <sup>d</sup>	0.002	0.250	0.016	

<sup>a</sup>In cases with resolution.

<sup>b</sup>Mann-Whitney U test.

<sup>c</sup>Fisher's exact test.

<sup>d</sup>Wilcoxon signed-rank test.

obtain the overall corneal NV score (range 0–12) for each eye. The scores of the two observers were then averaged and recorded as the clinical NV score of each eye. For quantification of the CD31-stained area, digital fluorescence pictures of the CD31-stained corneal flat mounts were analyzed using ImageJ software (National Institutes of Health, Bethesda, MD)<sup>26,58</sup>. The total area of the cornea was manually delineated by outlining the innermost vessels of the limbal arcade and erasing the area outside the total area. After background subtraction and thresholding, the percentage of CD31<sup>+</sup> area within the total corneal area was calculated. The measurements were performed by two independent researchers (J.Y.O. and H.J.L.) in a blinded manner, and the average values were used for analysis.

### HUVEC culture and angiogenesis assays

Angiogenesis assays on HUVECs (cat. no. C2519A, Lonza, Basel, Switzerland) cultured in EBM<sup>TM</sup>-2 Endothelial Cell Growth Basal Medium-2 (Lonza) containing 1% (vol/vol) fetal bovine serum (FBS, Gibco, Thermo Fisher Scientific, Waltham, MA, USA) and 1% penicillin/streptomycin (Gibco) were performed.

For the tube formation assay, HUVECs were placed on Matrigel (Corning, Corning, NY)-coated culture dishes and treated with 1–5000 µg/mL of moxifloxacin for 12 h. The degree of tube formation was quantified by counting the number of nodes of vascular tubes in randomly selected ×100 fields under an inverted microscope. For the migration assay, HUVECs were placed on gelatin-coated culture dishes. After 24 h, parts of the cells were excised with a blade. The degree of cell migration was quantified by counting the number of cells beyond the reference line at 12 h after treatment with 1–5000 µg/mL of moxifloxacin. For the viability assay, HUVECs were treated with 1–5000 µg/mL of moxifloxacin for 12 h. Cell viability was quantified using the EZ-CYTOX cell viability assay kit (DoGenBio, Seoul, Korea) according to the manufacturer's instructions.

### Immune cell culture and LPS stimulation assay

Splenocytes were isolated from C57BL6/N mouse spleens and primarily cultured in RPMI-1640 media (WELGENE, Gyeongsan, Korea) containing 5% (vol/vol) FBS (Gibco) and 1% penicillin/streptomycin (Sigma-Aldrich). THP-1 cells were purchased from a cell bank at Seoul National University Hospital, differentiated into macrophages by treatment with 300 ng/mL phorbol 12-myristate-13-acetate (PMA, tlr-pma, InvivoGen, San Diego, CA) for 3 h, and cultured in RPMI1640 media (WELGENE) containing 2% (vol/vol) heat-inactivated FBS (Gibco) and 1% penicillin/streptomycin (Sigma-Aldrich).

For the LPS stimulation assay, the cells were treated with 100 or 1000 ng/mL LPS (InvivoGen) and 0.05 mM β-mercaptoethanol for 18 h.

### Apoptosis assay

For the purposes of the apoptosis analysis, splenocytes and macrophages were stained with ANX and PI (FITC Annexin V Apoptosis Detection Kit I, BD Pharmingen) and assessed for ANX<sup>+</sup>PI<sup>+</sup> and ANX<sup>+</sup>PI<sup>-</sup> cells by flow cytometry (S1000EXi Flow Cytometer, Stratifiedigm, San Jose, CA). The data were analyzed using the FlowJo program (Tree Star, Ashland, OR).

### Phagocytosis assay

For phagocytic activity measurement, a BioParticle uptake assay was conducted (Vibrant<sup>TM</sup> Phagocytosis Assay Kit, Molecular Probes, Thermo Fisher Scientific, Waltham, MA). In brief, THP-1-differentiated macrophages were incubated in fluorescent BioParticle suspension (lyophilized particles from sacrificed *E. coli* strain K-12) for 2 h. The cells were then washed with PBS and quenched with trypan blue. The fluorescence was read on a plate reader.

### Real-time RT-PCR

The corneas were cut into small pieces by microscissors, lysed in RNA isolation reagent (RNA Bee, Tel-Test, Friendswood, TX), and homogenized with an ultrasound sonicator (Ultrasonic Processor, Cole Parmer Instruments, Vernon Hills, IL). Total RNA was extracted using the RNeasy Mini kit (Qiagen, Valencia, CA) and converted to first-strand cDNA by reverse transcription (High Capacity RNA-to-cDNA<sup>TM</sup> Kit, Applied Biosystems, Carlsbad, CA). Real-time RT-PCR was performed using specific TaqMan<sup>®</sup> probes for *Mpo*, *Tnfa*, *Il1b*, *Il6*, *Mmp9*, *Ang2*, *Cd31*, *Vegfa*, and *Vegfc* amplification and TaqMan<sup>®</sup> Universal PCR Master Mix (all from Applied Biosystems) in an automated instrument (ABI 7500 Real Time PCR System, Applied Biosystems). The assays were performed in dual technical replicates for each biological sample. The data were normalized to GAPDH and expressed as fold changes relative to the controls.

### ELISA

The cell-free supernatants were collected from cultures of THP-1-differentiated macrophages after centrifugation and analyzed for concentrations of TNF-α (DY210, Human TNF-α DuoSet ELISA), IL-1β (DY201, Human IL-1β DuoSet ELISA), IL-6 (DY206, Human IL-6 DuoSet ELISA), IL-10 (DY217B, Human IL-10 DuoSet ELISA), AREG (DY262, Human Amphiregulin DuoSet ELISA), active TGF-β1 (DY240, Human TGF-β1 DuoSet ELISAs), active TGF-β2 (DY302, Human TGF-β2 DuoSet ELISA), and PGE2 (KGE004B, Prostaglandin E2 Parameter Assay Kit)(all from R&D Systems, Minneapolis, MN).

The MMP-9 protein level was measured in the cornea by ELISA. For protein extraction, the corneas were minced into small pieces, lysed in RIPA buffer (Biosesang, Seongnam, Korea) containing Halt<sup>TM</sup> Protease Inhibitor Cocktail (Thermo Fisher Scientific), and sonicated on ice using an ultrasound sonicator. After centrifugation, the supernatant was acquired and assayed by MMP-9 ELISA kit (DY6718, Mouse Total MMP-9 DuoSet ELISA, R&D Systems).

The minimum protein levels of detection calculated from the standard curves were as follows: 3.9 pg/mL for IL-1β, 9.4 pg/mL for IL-6, 15.6 pg/mL for TNF-α and AREG, 31.2 pg/mL for IL-10, TGF-β1 and TGF-β2, 39.0 pg/mL for PGE2, and 78.1 pg/mL for MMP-9.

### Flow cytometry

For preparation of single cell suspensions, the spleen and DLNs were minced between the frosted ends of two glass slides, filtered through a 40 µm cell strainer (Corning), and centrifuged. Blood cells were acquired

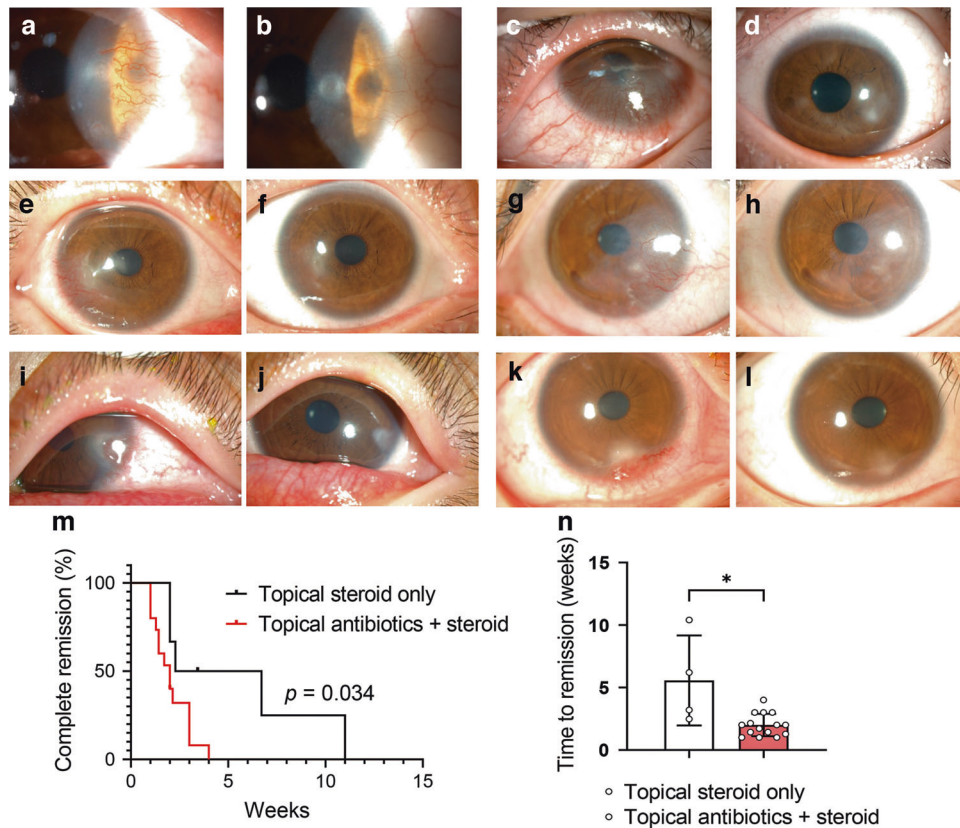


**Fig. 6 Topical antibiotics induce faster remission in patients with non-infectious marginal keratitis.** **a–l** Representative anterior segment photographs of patients with non-infectious marginal keratitis characterized by corneal new vessel ingrowth and inflammatory infiltration. Relative to before treatment (**a, c, e, g, i, k**), corneal new vessels regressed and infiltrations disappeared after topical antibiotic/corticosteroid treatment (**b, d, f, h, j, l**). Kaplan-Meier plots of cumulative complete remission probabilities according to treatment (**m**) and direct comparison of remission time between two treatment groups (**n**). Both the median and mean periods from treatment initiation to remission were significantly shorter in patients receiving combined antibiotic/steroid treatment than in those receiving topical steroid only. Mean values  $\pm$  SD are shown.  $p = 0.034$  by log-rank test,  $*p < 0.05$  by Mann-Whitney U test.

from the peripheral whole blood and treated with RBC lysis solution (Invitrogen). BM cells were isolated by flushing the BM of the femur and tibia and filtering them through a 70  $\mu$ m cell strainer (Corning). The resultant cell suspensions were centrifuged and subjected to staining.

The cells were stained with PE-Cy7 anti-CD11b [M1/70], Percp-Cy5.5 anti-Ly6C [HK1.4], FITC anti-Ly6G [1A8-Ly6g], PE-Cy7 anti-CD4 [GK1.5], PE anti-CD25 [PC61.5], APC anti-Foxp3 [FJK-16s], APC anti-MHC class II [M5/114.15.2], or APC anti-CD80 [16-10A1] antibodies (all from eBioscience, San Diego, CA). For Foxp3 staining, the cells were treated with Foxp3/Transcription Factor Fixation/Permeabilization Concentrate and Diluent solution (Invitrogen). The stained cells were assayed for fluorescence using a S1000EXi Flow Cytometer (Stratagene). The data were analyzed using the FlowJo program (Tree Star).

### Clinical study

To determine the therapeutic effect of topical antibiotic treatment in patients with non-infectious corneal inflammatory NV, we investigated a cohort of 117 pediatric patients (aged 15 years and younger) with non-infectious marginal keratitis at Seoul National University Hospital (Seoul, Korea) and Seoul National University Bundang Hospital (Seongnam, Korea) under the auspices of the Institutional Review Board of Seoul National University Hospital (IRB No. 2003-200-1112). The patients were divided into two groups: one treated with topical corticosteroid alone and the other with topical antibiotic/corticosteroid combination therapy. The patients treated with this combination therapy were 1:3 matched with the closest-propensity patients with topical corticosteroid monotherapy (i.e., those without antibiotic treatment) according to age, sex, and disease severity at disease onset. The rate of complete remission (i.e., complete regression of corneal new vessels and resolution of corneal infiltrates), time to remission, follow-up period and best-corrected visual acuity as well as demographic and ocular data were

collected from patients' medical records and anterior-segment photographs, and analyzed.

### Statistical analysis

All animals, experimental units and data points were included in the analysis. Prism software (GraphPad, San Diego, CA) was used for statistical test and generation of graphs. The D'Agostino & Pearson test or Shapiro-Wilk test was used to test for a normal distribution of data in each group. One-way ANOVA with Tukey's test or the Kruskal-Wallis test with Dunn's multiple-comparisons test was applied for comparison of the mean values from more than two groups. The Student's *t* test, Mann-Whitney *U* test and Fisher's exact test were used for comparison of continuous or categorical variables between the two groups. The Wilcoxon signed-rank test was used to compare visual acuities between pre-treatment and post-treatment in the same patient. Kaplan-Meier survival curves and the log-rank test were applied to determine and compare the time to complete remission in non-infectious keratitis patients. The data are presented as mean  $\pm$  SD, and differences were considered significant at  $p < 0.05$ . All available data are presented in the paper, and microbiome raw data can be provided upon request.

### REFERENCES

1. Belkaid, Y. & Hand, T. W. Role of the microbiota in immunity and inflammation. *Cell* **157**, 121–141 (2014).
2. Belkaid, Y. & Harrison, O. J. Homeostatic immunity and the microbiota. *Immunity* **46**, 562–576 (2017).
3. Thursby, E. & Juge, N. Introduction to the human gut microbiota. *Biochem. J.* **474**, 1823–1836 (2017).
4. Durack, J. & Lynch, S. V. The gut microbiome: relationships with disease and opportunities for therapy. *J. Exp. Med.* **216**, 20–40 (2019).

5. Fan, Y. & Pedersen, O. Gut microbiota in human metabolic health and disease. *Nat. Rev. Microbiol.* **19**, 55–71 (2021).
6. Trujillo-Vargas, C. M. et al. The gut-eye-lacrimal gland-microbiome axis in Sjögren syndrome. *Ocul. Surf.* **18**, 335–344 (2020).
7. Cavuoto, K. M., Banerjee, S. & Galor, A. Relationship between the microbiome and ocular health. *Ocul. Surf.* **17**, 384–392 (2019).
8. Zaheer, M. et al. Protective role of commensal bacteria in Sjögren Syndrome. *J. Autoimmun.* **93**, 45–56 (2018).
9. Horai, R. et al. Microbiota-dependent activation of an autoreactive T cell receptor provokes autoimmunity in an immunologically privileged site. *Immunity* **43**, 343–353 (2015).
10. Nakamura, Y. K. et al. Gut microbial alterations associated with protection from autoimmune uveitis. *Invest. Ophthalmol. Vis. Sci.* **57**, 3747–3758 (2016).
11. Liu, J. et al. Antibiotic-induced dysbiosis of gut microbiota impairs corneal nerve regeneration by affecting CCR2-negative macrophage distribution. *Am. J. Pathol.* **188**, 2786–2799 (2018).
12. Wu, M. et al. Antibiotic-induced dysbiosis of gut microbiota impairs corneal development in postnatal mice by affecting CCR2 negative macrophage distribution. *Mucosal Immunol.* **13**, 47–63 (2020).
13. Kugadas, A., Wright, Q., Geddes-McAlister, J. & Gadjeva, M. Role of microbiota in strengthening ocular mucosal barrier function through secretory IgA. *Investig. Ophthalmol. Vis. Sci.* **58**, 4593–4600 (2017).
14. Turnbaugh, P. J. et al. The human microbiome project. *Nature* **449**, 804–810 (2007).
15. Human Microbiome Project Consortium. Structure, function and diversity of the healthy human microbiome. *Nature* **486**, 207–214 (2012).
16. Human Microbiome Project Consortium. A framework for human microbiome research. *Nature* **486**, 215–221 (2012).
17. Dong, Q. et al. Diversity of bacteria at healthy human conjunctiva. *Investig. Ophthalmol. Vis. Sci.* **52**, 5408–5413 (2011).
18. Doan, T. et al. Paucibacterial microbiome and resident DNA virome of the healthy conjunctiva. *Invest. Ophthalmol. Vis. Sci.* **57**, 5116–5126 (2016).
19. Ozkan, J. et al. Temporal stability and composition of the ocular surface microbiome. *Sci. Rep.* **7**, 9880 (2017).
20. Kugadas, A. & Gadjeva, M. Impact of microbiome on ocular health. *Ocul. Surf.* **14**, 342–349 (2016).
21. Aragona, P. et al. The ocular microbiome and microbiota and their effects on ocular surface pathophysiology and disorders. *Surv. Ophthalmol.* **66**, 907–925 (2021).
22. Ozkan, J. & Willcox, M. D. The ocular microbiome: molecular characterisation of a unique and low microbial environment. *Curr. Eye Res.* **44**, 685–694 (2019).
23. Gomes, J. Á. P., Frizon, L. & Demeda, V. F. Ocular surface microbiome in health and disease. *Asia Pac. J. Ophthalmol. (Philos.)* **9**, 505–511 (2020).
24. Cursiefen, C. et al. VEGF-A stimulates lymphangiogenesis and hemangiogenesis in inflammatory neovascularization via macrophage recruitment. *J. Clin. Invest.* **113**, 1040–1050 (2004).
25. Cao, R. et al. Mouse corneal lymphangiogenesis model. *Nat. Protoc.* **6**, 817–826 (2011).
26. Song, H. B. et al. Mesenchymal stromal cells inhibit inflammatory lymphangiogenesis in the cornea by suppressing macrophage in a TSG-6-dependent manner. *Mol. Ther.* **26**, 162–172 (2018).
27. Gurung, H. R., Carr, M. M., Bryant, K., Chucuir-Elliott, A. J. & Carr, D. J. Fibroblast growth factor-2 drives and maintains progressive corneal neovascularization following HSV-1 infection. *Mucosal Immunol.* **22**, 172–185 (2018).
28. Xu, J. et al. The effect of different combinations of antibiotic cocktails on mice and selection of animal models for further microbiota research. *Appl. Microbiol. Biotechnol.* **105**, 1669–1681 (2021).
29. Miyake, H. et al. Toxicities of and inflammatory responses to moxifloxacin, cefuroxime, and vancomycin on retinal vascular cells. *Sci. Rep.* **9**, 9745 (2019).
30. Dalhoff, A. & Shalit, I. Immunomodulatory effects of quinolones. *Lancet Infect. Dis.* **3**, 359–371 (2003).
31. Qiu, Z. et al. Bidirectional effects of moxifloxacin on the pro-inflammatory response in lipopolysaccharide-stimulated mouse peritoneal macrophages. *Mol. Med. Rep.* **18**, 5399–5408 (2018).
32. Potente, M., Gerhardt, H. & Carmeliet, P. Basic and therapeutic aspects of angiogenesis. *Cell* **146**, 873–887 (2011).
33. Yang, T. et al. Daphnetin inhibits corneal inflammation and neovascularization on a mouse model of corneal alkali burn. *Int. Immunopharmacol.* **103**, 108434 (2022).
34. Li, Q. et al. Dasatinib loaded nanostructured lipid carriers for effective treatment of corneal neovascularization. *Biomater. Sci.* **9**, 2571–2583 (2021).
35. Xu, K. et al. DCZ3301, an aryl-guanidino agent, inhibits ocular neovascularization via PI3K/AKT and ERK1/2 signaling pathways. *Exp. Eye Res.* **201**, 108267 (2020).
36. Wan, S. S., Pan, Y. M., Yang, W. J., Rao, Z. Q. & Yang, Y. N. Inhibition of EZH2 alleviates angiogenesis in a model of corneal neovascularization by blocking FoxO<sub>3a</sub>-mediated oxidative stress. *FASEB J.* **34**, 10168–10181 (2020).
37. Tang, M. et al. Tetramethylpyrazine in a murine alkali-burn model blocks NFκB/NRF-1/CXCR4-signaling-induced corneal neovascularization. *Investig. Ophthalmol. Vis. Sci.* **59**, 2133–2141 (2018).
38. Garreis, F., Gottschalt, M. & Paulsen, F. P. Antimicrobial peptides as a major part of the innate immune defense at the ocular surface. *Dev. Ophthalmol.* **45**, 16–22 (2010).
39. Mantelli, F. & Argüeso, P. Functions of ocular surface mucins in health and disease. *Curr. Opin. Allergy Clin. Immunol.* **8**, 477–483 (2008).
40. Mantelli, F., Mauris, J. & Argüeso, P. The ocular surface epithelial barrier and other mechanisms of mucosal protection: from allergy to infectious diseases. *Curr. Opin. Allergy Clin. Immunol.* **13**, 563–568 (2013).
41. Martínez-Carrasco, R., Argüeso, P. & Fini, M. E. Membrane-associated mucins of the human ocular surface in health and disease. *Ocul. Surf.* **21**, 313–330 (2021).
42. Ueta, M. & Kinoshita, S. Ocular surface inflammation is regulated by innate immunity. *Prog. Retin. Eye Res.* **31**, 551–575 (2012).
43. Galletti, J. G., Guzmán, M. & Giordano, M. N. Mucosal immune tolerance at the ocular surface in health and disease. *Immunology* **150**, 397–407 (2017).
44. Heissigerova, J. et al. The microbiota determines susceptibility to experimental autoimmune uveoretinitis. *J. Immunol. Res.* **2016**, 5065703 (2016).
45. Richardson, R. & Bhela, S. Gut bacteria modulates angiogenesis and corneal immunopathology after herpes simplex virus infection. *J. Immunol.* **190**, 128.19 (2013).
46. Sato, S. et al. Positive effects of oral antibiotic administration in murine chronic graft-versus-host disease. *Int. J. Mol. Sci.* **22**, 3745 (2021).
47. Andriessen, E. M. et al. Gut microbiota influences pathological angiogenesis in obesity-driven choroidal neovascularization. *EMBO Mol. Med.* **8**, 1366–1379 (2016).
48. Kugadas, A. et al. Impact of microbiota on resistance to ocular pseudomonas aeruginosa-induced keratitis. *PLoS Pathog.* **12**, e1005855 (2016).
49. Papa, V. et al. Treatment of acute bacterial conjunctivitis with topical netilmicin. *Cornea* **21**, 43–47 (2002).
50. Kim, S. J. & Toma, H. S. Ophthalmic antibiotics and antimicrobial resistance a randomized, controlled study of patients undergoing intravitreal injections. *Ophthalmology* **118**, 1358–1363 (2011).
51. Dave, S. B., Toma, H. S. & Kim, S. J. Changes in ocular flora in eyes exposed to ophthalmic antibiotics. *Ophthalmology* **120**, 937–941 (2013).
52. Yin, V. T. et al. Antibiotic resistance of ocular surface flora with repeated use of a topical antibiotic after intravitreal injection. *JAMA Ophthalmol.* **131**, 456–461 (2013).
53. Venugopal, R. et al. Conjunctival microbial flora in ocular stevens-johnson syndrome sequelae patients at a tertiary eye care center. *Cornea* **35**, 1117–1121 (2016).
54. Doan, T. et al. Post-antibiotic ocular surface microbiome in children: a cluster-randomized trial. *Ophthalmology* **127**, 1127–1130 (2020).
55. Petrillo, F. et al. Current evidence on the ocular surface microbiota and related diseases. *Microorganisms* **8**, 1033 (2020).
56. Yoon, C. H., Ryu, J. S., Moon, J. & Kim, M. K. Association between aging-dependent gut microbiome dysbiosis and dry eye severity in C57BL/6 male mouse model: a pilot study. *BMC Microbiol.* **21**, 106 (2021).
57. Anderson, C., Zhou, Q. & Wang, S. An alkali-burn injury model of corneal neovascularization in the mouse. *J. Vis. Exp.* **86**, 51159 (2014).
58. Rabiolo, A., Bignami, F., Rama, P. & Ferrari, G. Vessel: a new tool for semiautomatic measurement of corneal neovascularization. *Investig. Ophthalmol. Vis. Sci.* **56**, 8199–8206 (2015).

## ACKNOWLEDGEMENTS

This work was supported by the National Research Foundation of Korea (2021R1A2C3004532 to J.Y.O. and 2018M3D1A1058826 to J.H.K.) and by Creative-Pioneering Researchers Program through Seoul National University (to D.K.). We appreciate Dr. Hyun Sun Jeon (Seoul National University Bundang Hospital) for assistance with clinical study and Dr. Sang-Taek Im (FARB Laboratory) for assistance with angiogenesis assays.

## AUTHOR CONTRIBUTIONS

Conceptualization: J.Y.O. Methodology: H.J.L., C.H.Y., H.J.K., J.H.K. (Jung Hwa Ko), J.S.R., D.H.J., J.H.K. (Jeong Hun Kim), D.K. and J.Y.O. Investigation: H.J.L., C.H.Y., H.J.K., J.H.K. (Jung Hwa Ko), J.S.R. and J.Y.O. Visualization: H.J.L., C.H.Y. and J.Y.O. Funding acquisition: J.H.K. (Jeong Hun Kim), D.K. and J.Y.O. Project administration: J.H.K. (Jung Hwa Ko) and J.Y.O. Supervision: J.Y.O. Writing—original draft: H.J.L., C.H.Y., J.H.K. (Jung Hwa Ko), J.S.R., D.H.J. and J.Y.O. Writing—review & editing: D.K. and J.Y.O. H.J.L.

and C.H.Y. contributed equally (H.J.L. contributed to Figs. 1, 2, S1 and S2; C.H.Y. contributed to Figs. 3, 6, S3 and Table 1).

### COMPETING INTERESTS

The authors have declared that no conflict of interest exists.

### ADDITIONAL INFORMATION

**Supplementary information** The online version contains supplementary material available at <https://doi.org/10.1038/s41385-022-00555-2>.

**Correspondence** and requests for materials should be addressed to Joo Youn Oh.

**Reprints and permission information** is available at <http://www.nature.com/reprints>

**Publisher's note** Springer Nature remains neutral with regard to jurisdictional claims in published maps and institutional affiliations.

Springer Nature or its licensor holds exclusive rights to this article under a publishing agreement with the author(s) or other rightsholder(s); author self-archiving of the accepted manuscript version of this article is solely governed by the terms of such publishing agreement and applicable law.